

Physics Updates from HERMES

Morgan J. Murray on behalf of the HERMES Collaboration

Rm. 514b, Dept. of Physics & Astronomy, University of Glasgow, Glasgow, G12 8QQ, Scotland

Abstract. The HERMES collaboration presents two sets of recent results: the first related to an extraction of the g_2 nucleon structure function determined for DIS on a polarised target and the second related to the measurement of asymmetries related to the deeply virtual Compton scattering process that can be used to discover information on generalised parton distributions and hence nucleon structure.

Keywords: lepton-nucleon scattering, nucleon structure, structure functions, generalised parton distributions

PACS: 13.40.Gp, 13.85.Hd, 14.20.Dh, 13.85.Hd

THE HERMES EXPERIMENT

The HERMES experiment was a fixed-target experiment on the HERA ring in Hamburg, Germany. The experiment ran from 1995-2007 and used the electron/positron beam made available by the HERA accelerator. A variety of polarised targets were used; the targets under consideration in these proceedings were transversely polarised (w.r.t. the beam direction) and polarisation averaged proton targets.

EXTRACTION OF THE g_2 STRUCTURE FUNCTION

Experimental Details

The F_1 , F_2 and g_1 structure functions are well-known quantities in the field of nucleon structure physics. Much less is known about the g_2 structure function, which (unlike the aforementioned functions) has no intuitively-graspable interpretation as a probability density. Compared to its brother-functions, g_2 (and its related asymmetry A_2) has undergone relatively little experimental scrutiny. There have been some prior experimental extractions of g_2 at SLAC and CERN [1, 2, 3]. The former facility has observed evidence of unexpected potential twist-3 behaviour, i.e. they deviate from the twist-3 behaviour calculated using the Wandzura-Wilczek approximation.

The A_2 asymmetry and g_2 distribution were extracted at HERMES from data taken in 2003-2005 [4], when a transversely polarised Hydrogen gas target was used in the experiment. The target has an average polarisation of 78% and the electron/positron beam was polarised to approximately 34%. The applied kinematic boundaries for the accumulated data set were $0.18\text{GeV}^2 < Q^2 < 20\text{GeV}^2$, $W > 1.8\text{GeV}$, $0.004 < x < 0.9$ and $0.10 < y < 0.91$. The data were corrected for the charge-symmetric e^+e^- background, which amounted in total to about 1.8% of the events, reaching the largest

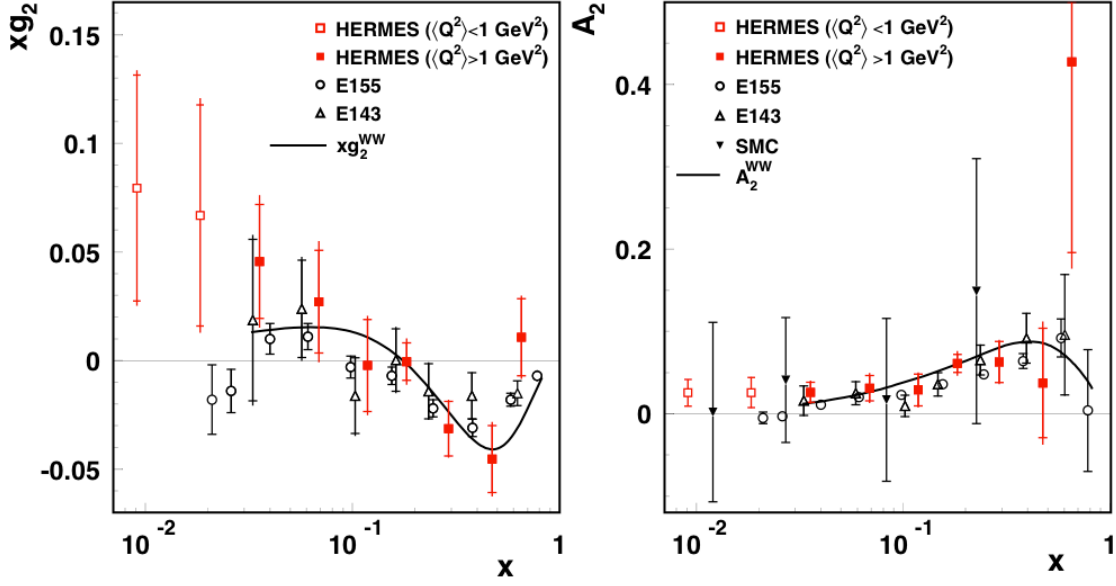


FIGURE 1. Values of g_2 (left) and A_2 (right) extracted at HERMES (red squares) in two bins of Q^2 and projected along x . The results are compared to previous measurements taken at SLAC and CERN and a Wandzura-Wilczek calculation of twist-3 effects. Inner error bars are the statistical uncertainties; outer bars are the statistical and systematic uncertainties added in quadrature.

contribution of about 14% at small values of x . The asymmetry

$$A_{LT}(x, Q^2, \phi, h_\ell) = h_\ell \frac{N^{h_\ell \uparrow}(x, Q^2, \phi) \mathcal{L}^{h_\ell \downarrow} - N^{h_\ell \downarrow}(x, Q^2, \phi) \mathcal{L}^{h_\ell \uparrow}}{N^{h_\ell \uparrow}(x, Q^2, \phi) \mathcal{L}_p^{h_\ell \downarrow} + N^{h_\ell \downarrow}(x, Q^2, \phi) \mathcal{L}_p^{h_\ell \uparrow}} \quad (1)$$

was measured in bins of x , Q^2 , and the azimuthal scattering angle ϕ where $N^{h_\ell \uparrow(\downarrow)}(x, Q^2, \phi)$ is the number of scattered leptons in each bin for the case of an incident lepton with helicity h_ℓ when the direction of the proton spin points up (down). The quantities $\mathcal{L}^{h_\ell \uparrow(\downarrow)}$ and $\mathcal{L}_p^{h_\ell \uparrow(\downarrow)}$ are the corresponding integrated luminosities and the integrated luminosities weighted with the absolute value of the beam and target polarization product, respectively. The measured asymmetries are corrected for radiative and instrumental smearing effects. The resultant data in each (x, Q^2) -bin were fit with a functional form of $A_T \cos \phi$ and A_2 and g_2 were calculated from A_T with knowledge of the F_2 and g_1 structure functions and $R(x, Q^2)$, the ratio of longitudinal to transverse virtual-photon absorption cross sections.

Result

The resultant values are shown in figure 1. The results from HERMES are split into two different bins in Q^2 and projected along x . The HERMES data is consistent with previous measurements, but not sufficiently precise to make conclusions about potential deviations from twist-2 behaviour. The results for g_2 are consistent with the Cottingham-

Burkardt sum rule [5], which states that for sufficiently large Q^2 the integral of g_2 over x should be zero.

EXCLUSIVE PHYSICS

Knowledge of nucleon structure can be expanded by considering generalised parton distributions (GPDs); access to GPDs can be achieved by measuring particle production in scattering processes where the target nucleon remains intact. The simplest process to measure is deeply virtual Compton Scattering (DVCS), where a photon is produced by a parton from the nucleon [6, 7, 8, 9, 10]. It is also possible to interpret measurements of produced mesons in the GPD framework, e.g. [11, 12, 13, 14]. The HERMES experiment recently produced DVCS measurements from the entire 1995-2007 data set, where beam helicity and charge azimuthal asymmetries in the produced particle distributions are measured, see figures 2 and 3 respectively. The HERMES experiment can distinguish the pure DVCS contribution to the asymmetries from the contribution due to the interference with the competing Bethe-Heitler process due to the presence of both beam charges in the data set. These measurements are taken with a missing-mass selection technique, where the target nucleon scatters outside the HERMES geometric acceptance and must be reconstructed from measurements of the produced photon and scattered lepton. This event selection technique allows a certain amount of background into the data sample, mostly from events involving a resonant state of the target nucleon. The collaboration has also published measurements from an kinematically completely reconstructed data sample [15] that was taken with additional experimental equipment—the beam helicity asymmetry measured using an exclusive event selection technique is shown in figure 4. Unfortunately, there is only a single beam charge available for this additional dataset, so it is not possible to distinguish between the contributions from the interference and $|\text{DVCS}|^2$ terms to the asymmetry. It is, however, possible to make a first extraction of the beam helicity asymmetry associated with the resonant events that contaminate the missing-mass selected data sample. The beam helicity asymmetry for the process $ep \rightarrow e\Delta\gamma \rightarrow ep\pi^0\gamma$ is shown in figure 5.

ACKNOWLEDGMENTS

We gratefully acknowledge the DESY management for its support, the staff at DESY and the collaborating institutions for their significant effort, and our national funding agencies and the EU FP7 (HadronPhysics2, Grant Agreement number 227431) for financial support.

REFERENCES

1. E143 Coll., K. Abe et al., *Phys. Rev. D* **58** (1998) 112003.
2. E155 Coll., P. L. Anthony et al., *Phys. Lett. B* **553** (2003) 18.
3. SMC Coll., D. Adams et al., *Phys. Rev. D* **56** (1997) 5330.
4. A. Airapetian et al., *Eur. Phys. J. C* **72** (2012) 1921.

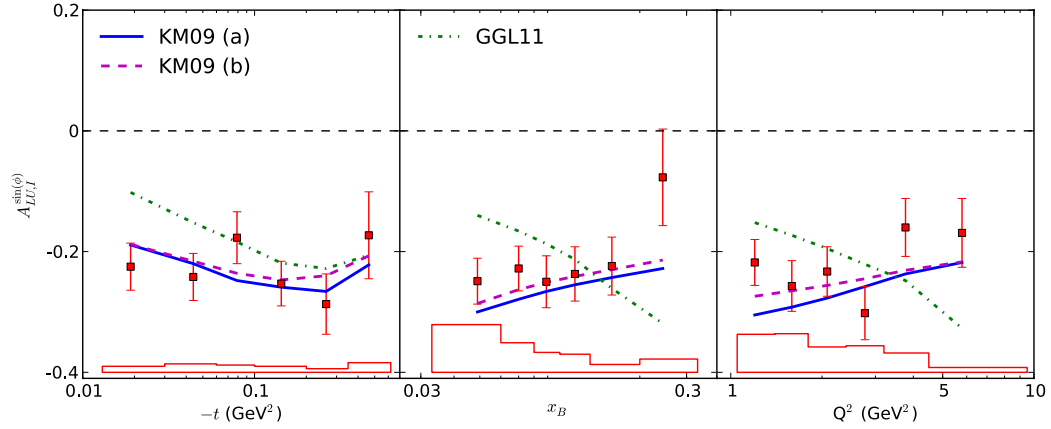


FIGURE 2. The interference contribution to the first harmonic of the beam helicity asymmetry projected in six bins along the three kinematic dimensions $-t$, x_B and Q^2 . This measurement can be used to constrain a part of the GPD H , the generalised parton distribution that reduces to the parton distribution $q(x)$ in its forward limit. Error bars are the statistical uncertainties; error bands are the systematic uncertainties. The curves on the figure come from [16] and [17].

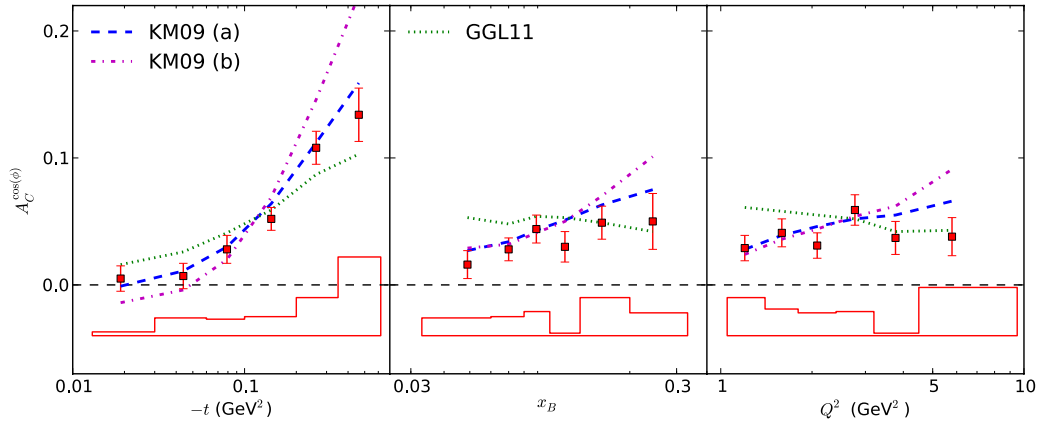


FIGURE 3. The DVCS and interference contributions to the first harmonic of the beam charge asymmetry. This measurement can be used to constrain a part of the GPD H , the generalised parton distribution that reduces to the parton distribution $q(x)$ in its forward limit. The curves on the figure come from [16] and [17].

5. H. Burkhardt and W.N. Cottingham, *Ann. Phys.* **56** (1970) 453.
6. A. Airapetian et al., *JHEP* **07** (2012) 032.
7. A. Airapetian et al., *JHEP* **11** (2009) 083.
8. A. Airapetian et al., *Phys. Lett.* **B 704** (2011) 15-23.
9. A. Airapetian et al., *JHEP* **06** (2010) 019.
10. A. Airapetian et al., *JHEP* **06** (2008) 066.
11. A. Airapetian et al., *Eur. Phys. J. C* **62** (2009) 659-694.
12. A. Airapetian et al., *Phys. Lett.* **B 679** (2009) 100-105.
13. A. Airapetian et al., *Phys. Lett.* **B 682** (2010) 345-350.

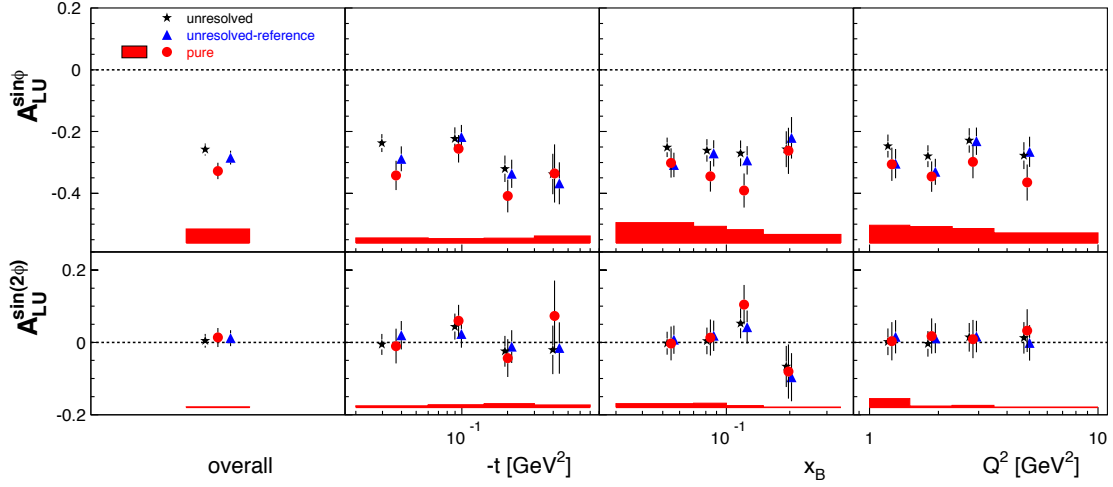


FIGURE 4. The beam helicity asymmetry measured using a missing-mass event selection technique in the original HERMES acceptance (black), in the HERMES acceptance as modified by the installation of the recoil detector (blue) and with a highly pure exclusive event selection technique (red). The first harmonic shows that a pure sample has a slightly larger asymmetry value at the larger $-t$ values associated with high contamination in the missing-mass selected sample by resonant events. The second harmonic is compatible with zero.

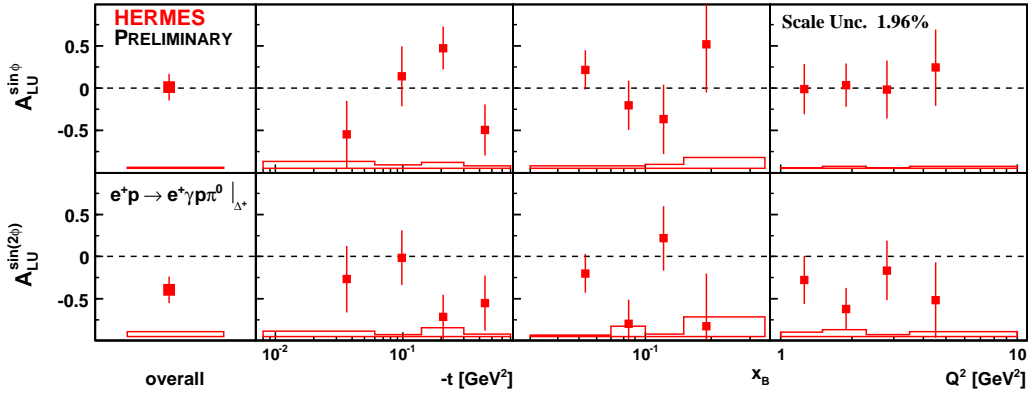


FIGURE 5. The beam helicity asymmetry associated with the process $ep \rightarrow e\Delta\gamma \rightarrow ep\pi^0\gamma$, which is partly responsible for a 12% contamination of the missing-mass selected data sample. The amplitude of the asymmetry is compatible with zero.

14. A. Airapetian et al., *Eur. Phys. J. C* **71** (2011) 1609.
15. A. Airapetian et al., *JHEP* **10** (2012) 042.
16. K. Kumerički and D. Müller, *Nucl. Phys. B* **841** (2010) 1.
17. G. Goldstein, J. Hernandez and S. Liuti, *Phys. Rev. D* **84** (2011) 034007.